Original Article | Gastrointestinal Imaging

eISSN 2005-8330
https://doi.org/10.3348/kjr.2022.0494
Korean J Radiol 2022;23(12):1269-1280

Korean Journal of Radiology
KJR

Prediction of Decompensation and Death in Advanced Chronic Liver Disease Using Deep Learning Analysis of Gadoxetic Acid-Enhanced MRI

Subin Heo[1, 2], Seung Soo Lee[1], So Yeon Kim[1], Young-Suk Lim[3], Hyo Jung Park[1], Jee Seok Yoon[4], Heung-Il Suk[4, 5], Yu Sub Sung[6], Bumwoo Park[7], Ji Sung Lee[8]

[1]Department of Radiology and Research Institute of Radiology, Asan Medical Center, University of Ulsan College of Medicine, Seoul, Korea; [2]Department of Radiology, Ajou University School of Medicine, Suwon, Korea; [3]Department of Gastroenterology, Liver Center, Asan Medical Center, University of Ulsan College of Medicine, Seoul, Korea; Departments of [4]Brain and Cognitive Engineering and [5]Artificial Intelligence, Korea University, Seoul, Korea; [6]Clinical Research Center, Asan Medical Center, Seoul, Korea; [7]Health Innovation Big Data Center, Asan Institute for Life Sciences, Asan Medical Center, Seoul, Korea; [8]Department of Clinical Epidemiology and Biostatistics, Asan Medical Center, University of Ulsan College of Medicine, Seoul, Korea

Objective: This study aimed to evaluate the usefulness of quantitative indices obtained from deep learning analysis of gadoxetic acid-enhanced hepatobiliary phase (HBP) MRI and their longitudinal changes in predicting decompensation and death in patients with advanced chronic liver disease (ACLD).

Materials and Methods: We included patients who underwent baseline and 1-year follow-up MRI from a prospective cohort that underwent gadoxetic acid-enhanced MRI for hepatocellular carcinoma surveillance between November 2011 and August 2012 at a tertiary medical center. Baseline liver condition was categorized as non-ACLD, compensated ACLD, and decompensated ACLD. The liver-to-spleen signal intensity ratio (LS-SIR) and liver-to-spleen volume ratio (LS-VR) were automatically measured on the HBP images using a deep learning algorithm, and their percentage changes at the 1-year follow-up (ΔLS-SIR and ΔLS-VR) were calculated. The associations of the MRI indices with hepatic decompensation and a composite endpoint of liver-related death or transplantation were evaluated using a competing risk analysis with multivariable Fine and Gray regression models, including baseline parameters alone and both baseline and follow-up parameters.

Results: Our study included 280 patients (153 male; mean age ± standard deviation, 57 ± 7.95 years) with non-ACLD, compensated ACLD, and decompensated ACLD in 32, 186, and 62 patients, respectively. Patients were followed for 11–117 months (median, 104 months). In patients with compensated ACLD, baseline LS-SIR (sub-distribution hazard ratio [sHR], 0.81; $p = 0.034$) and LS-VR (sHR, 0.71; $p = 0.01$) were independently associated with hepatic decompensation. The ΔLS-VR (sHR, 0.54; $p = 0.002$) was predictive of hepatic decompensation after adjusting for baseline variables. ΔLS-VR was an independent predictor of liver-related death or transplantation in patients with compensated ACLD (sHR, 0.46; $p = 0.026$) and decompensated ACLD (sHR, 0.61; $p = 0.023$).

Conclusion: MRI indices automatically derived from the deep learning analysis of gadoxetic acid-enhanced HBP MRI can be used as prognostic markers in patients with ACLD.

Keywords: *Cirrhosis; Magnetic resonance imaging; Deep learning; Gadolinium methoxybenzyl DTPA*

INTRODUCTION

Compensated advanced chronic liver disease (cACLD), first introduced in the Baveno VI consensus, describes the spectrum of advanced fibrosis and cirrhosis in asymptomatic patients [1]. Although asymptomatic, patients with

Received: July 20, 2022 **Revised:** September 12, 2022 **Accepted:** October 11, 2022
Corresponding author: Seung Soo Lee, MD, PhD, Department of Radiology and Research Institute of Radiology, Asan Medical Center, University of Ulsan College of Medicine, 88 Olympic-ro 43-gil, Songpa-gu, Seoul 05505, Korea.
• E-mail: seungsoolee@amc.seoul.kr

cACLD are at risk of developing portal hypertension and decompensation, which are associated with increased liver-related mortality [2,3]. Therefore, identifying patients at risk of decompensation is important as they may benefit from enhanced surveillance and timely prophylactic measures. Prognostic prediction is also important in determining the timing of lifesaving treatments, such as transplantation, in patients with decompensated ACLD (dACLD).

MRI using a liver-specific contrast agent, gadoxetic acid (Eovist or Primovist; Bayer Health Care), has been used for the diagnosis and staging of hepatocellular carcinoma (HCC) because of its high sensitivity in HCC detection [4,5]. It is also considered an alternative method for HCC surveillance in high-risk patients and those with inadequate ultrasound examinations [6-8]. Additionally, gadoxetic acid-enhanced MRI may assess liver function because the degree of liver enhancement on hepatobiliary phase (HBP) images reflects hepatocyte uptake function [9-11]. The liver-to-spleen signal intensity (SI) ratio (LS-SIR) measured on HBP images was used as an index of functional liver capacity [11]. In contrast, image-based liver and spleen volumetry may have prognostic implications in patients with chronic liver disease. Furthermore, the liver-to-spleen volume ratio (LS-VR) has been suggested as an index for detecting clinically significant portal hypertension and hepatic decompensation [12-14]. Therefore, we hypothesized that functional (i.e., LS-SIR) and volumetric (i.e., LS-VR) indices measured using gadoxetic acid-enhanced MRI may be useful in the risk stratification of chronic liver disease.

A deep learning algorithm (DLA) has enabled the automated measurement of volumes and SIs of the liver and spleen using gadoxetic acid-enhanced MRI [11], which facilitates the clinical application of LS-SIR and LS-VR. If these indices can predict the prognosis of chronic liver disease, the use of a DLA could generate add-on information using routine gadoxetic acid-enhanced MRI without additional cost or effort. Because patients with chronic liver disease may undergo repeated MRI examinations, longitudinal changes in MRI-based indices may also be of clinical interest.

Therefore, this study aimed to measure LS-SIR and LS-VR using deep learning analysis of gadoxetic acid-enhanced HBP images and to evaluate the usefulness of these indices and their longitudinal changes in predicting hepatic decompensation and death in patients with ACLD.

MATERIALS AND METHODS

This study was approved by our Institutional Review Board, and the requirement for informed consent was waived because of the retrospective nature of the study (IRB No. 2021-1550).

Study Population

This study was a retrospective analysis of prospectively collected data (Surveillance of Patients with Cirrhosis at High Risk of HCC by MRI with Liver-Specific Contrast, PRIUS Study, ClinicalTrials.gov ID: NCT01446666) from a single tertiary institution in Korea [7]. The study population was recruited between November 2011 and August 2012 to compare HCC detection rates using ultrasound and gadoxetic acid-enhanced MRI as surveillance tests. The study population included patients aged ≥ 20 years with a high risk of developing HCC and no previous or current suspicion of HCC. HCC risk was estimated using the following model [7]: 1.41 (if age ≥ 50 years) + 1.65 (if prothrombin activity ≤ 75%) + 0.92 (if platelet count < 100 x 10^3/mm^3) + 0.74 (if positive anti-hepatitis C virus antibody or hepatitis B virus surface antigen), and a high risk of developing HCC was defined as a model score > 2.33. The patients underwent baseline clinical evaluation and one to three rounds of paired US and gadoxetic acid-enhanced MRI examinations at 6-month intervals.

Among the 407 patients enrolled in the original prospective study, we included those who completed the baseline and 1-year follow-up (i.e., the third round) MRI in this study. The exclusion criteria include incomplete coverage of the liver and spleen by MRI, HCC detected at baseline or during 1-year surveillance, missing baseline clinical data, and image data loss. We also excluded four patients in whom deep learning failed in spleen segmentation owing to spleen signal abnormality caused by Gamna-Gandy bodies.

Baseline Data Collection

Clinical and laboratory parameters, including demographic data, liver disease etiology, platelet count, serum albumin level, Model for End-Stage Liver Disease (MELD) score, and upper endoscopy findings (if available) were assessed at baseline. Liver stiffness (LS) was measured using a two-dimensional shear wave elastography unit (Supersonic Imagine) and an SC6-1 probe as described in previous studies [15,16]. Based on the presence of ACLD and previous or current hepatic decompensation, the baseline

https://doi.org/10.3348/kjr.2022.0494

Korean Journal of Radiology
KJR

state of liver disease for individual patients was categorized as non-ACLD, cACLD (ACLD without decompensation), or decompensated ACLD (dACLD; previous or current decompensation). ACLD was defined according to the Baveno VI criteria [1] and LS threshold for shear wave elastography proposed by the Society of Radiologists in Ultrasound Liver Elastography [17]. Patients were considered to have ACLD if they had an LS > 9 kPa, gastroesophageal varices on endoscopy, or pathologically proven advanced fibrosis or cirrhosis. Hepatic decompensation was defined as the occurrence of ascites, variceal bleeding, or grade ≥ 2 hepatic encephalopathy [18].

Measurement of MRI Indices Using a Deep Learning Algorithm

All MRI examinations were performed using a 1.5T scanner (Magnetom Avanto; Siemens). Fat-saturated axial T1-weighted HBP images were obtained 20 minutes after administering 0.025 mmol/kg of gadoxetic acid using a three-dimensional gradient-echo sequence (volume interpolated breath-hold examination; Siemens) with the following parameters: echo time, 1.46 ms; repetition time, 4.06 ms; flip angle, 10°; matrix, 320 x 220; field of view, 380 x 261 mm; and slice thickness and interval, 4 mm. The HBP MRI data for the baseline and 1-year follow-up examinations were analyzed. The HBP images were processed using a DLA for automated liver and spleen segmentation [11] implemented in the software (GoDCSS; SmartCareworks Inc.). The details of the algorithm were described in a previous study [11]. Briefly, the algorithm outlines liver and spleen margins on HBP images while excluding vessels or focal hepatic lesions, with a reported dice similarity score of 95%–98% [11]. After uploading the MRI data, the software automatically performed the liver and spleen segmentation. A board-certified radiologist (23 years of experience) reviewed the deep learning-generated segmentation results and corrected any segmentation errors using the software. The time required to correct the errors was recorded. The volume and SI of the whole liver and spleen were measured, and LS-SIR and LS-VR were calculated as liver SI divided by spleen SI and liver volume divided by spleen volume, respectively, for each MRI examination. The follow-up MRI indices (ΔLS-SIR and ΔLS-VR), representing the change in the LS-SIR and LS-VR between the baseline and 1-year follow-up MRI examinations, were calculated for each patient as "(the value at the 1-year follow-up MRI – the value at the baseline MRI)/the value at the baseline MRI x 100 (%)."

Follow-Up and Outcome Measurement

The baseline MRI date was considered the baseline time point. Patients were followed up until death, their last clinical visit, or the end of the follow-up period (2021-10-15). As the study outcomes, the occurrence of hepatic decompensation was assessed in the cACLD group, and the occurrence of liver-related death or liver transplantation was evaluated in the cACLD and dACLD groups. HCC development during the follow-up period was also recorded.

Statistical Analysis

Data are summarized as mean and standard deviation (SD) or median and interquartile range for continuous variables and frequency and percentage for categorical variables. Comparisons of baseline patient characteristics were conducted using the Kruskal–Wallis H test and analysis of variance for continuous variables and Fisher's exact test for categorical variables. The associations between MRI indices and hepatic decompensation in the cACLD group and a composite endpoint of liver-related death or transplantation in the cACLD and dACLD groups were evaluated using competing risk analysis with Fine and Gray regression models [19]. Any death or transplantation before decompensation was treated as a competing event for hepatic decompensation, and non-liver-related death was regarded as a competing event for liver-related death or transplantation. Following univariable analysis, multivariable analysis was performed using two models; the baseline multivariable model included baseline MRI indices (LS-SIR and LS-VR) and clinical variables alone that showed $p < 0.1$ at the univariable analysis, whereas the follow-up multivariable model included both follow-up MRI indices (ΔLS-SIR and ΔLS-VR) and the variables in the baseline multivariable model. The ΔLS-VR was categorized as < -13%, -13% to 13%, and > 13%, and a threshold of ± 13% was chosen based on the reported reproducibility range of MRI-based volume measurement in a previous study [20]. The optimal cutoff values for the other MRI indices were determined using the minimum Wald p value method in the Cox model [21]. The probability of outcome occurrence was estimated after accounting for competing events using the cumulative incidence function (CIF) method [22], and differences were tested using Gray's test [23]. Subsequently, the associations of MRI indices with liver-related outcomes adjusted for the effect of HCC development were evaluated

 https://doi.org/10.3348/kjr.2022.0494

using baseline and follow-up multivariable Fine and Gray regression models comprising HCC development as a time-dependent covariate. The agreement between the MRI indices automatically measured by DLA and those measured after the radiologist's correction was evaluated using the 95% Bland–Altman limit of agreement. Patient categorization results using the cutoff MRI index values were compared between the automatic measurements by DLA and the measurements after the radiologist's correction. Statistical significance was set at $p < 0.05$. Statistical analyses were performed using the SAS software (version 9.4; SAS Institute Inc.) and R (version 3.6.0; R Foundation for Statistical Computing).

RESULTS

Characteristics of the Study Population

This study included 280 patients (153 male and 127 female; mean age, 57 ± 7.95 years; age range, 29–74 years) (Fig. 1). Table 1 summarizes the baseline characteristics of the study participants. Non-ACLD, cACLD, and dACLD were observed in 32, 186, and 62 patients, respectively.

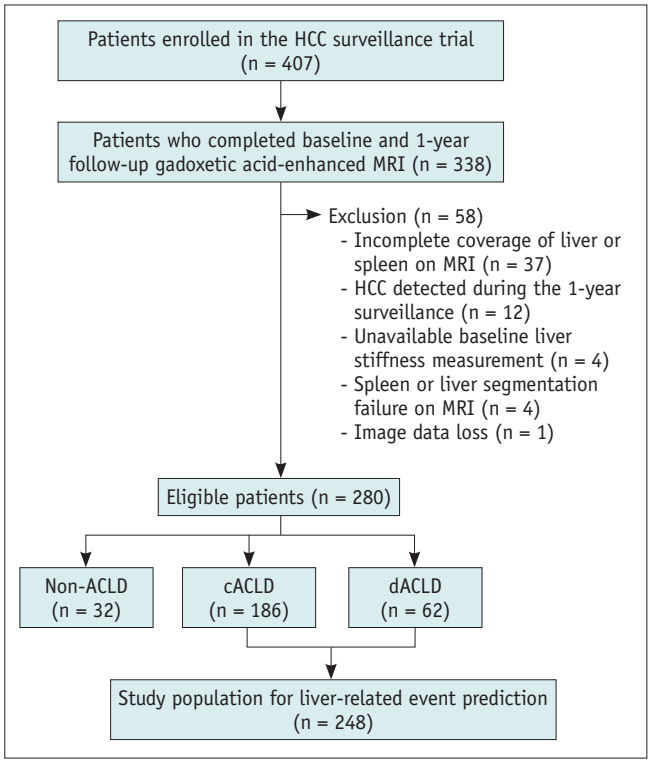

Fig. 1. Flow diagram of the study population. cACLD = compensated advanced chronic liver disease, dACLD = decompensated advanced chronic liver disease, HCC = hepatocellular carcinoma, Non-ACLD = non-advanced chronic liver disease

Although the liver disease etiology differed among the three groups ($p < 0.001$), hepatitis B was the most common etiology in the non-ACLD (26/32, 81.3%), cALCD (135/186, 72.6%), and dACLD (36/62, 58.1%) groups. The baseline LS-SIR (mean ± SD, 1.84 ± 0.21, 1.65 ± 0.22, and 1.52 ± 0.19, respectively; $p < 0.001$) and LS-VR (mean ± SD, 3.80 ± 2.33, 3.18 ± 1.91, and 2.00 ± 1.04, respectively; $p < 0.001$) values differed significantly among the non-ACLD, cALCD, and dACLD groups (Supplementary Fig. 1). However, ΔLS-SIR ($p = 0.942$) and ΔLS-VR ($p = 0.453$) showed no differences among the three groups. Significant differences were observed in platelet count ($p = 0.004$), serum albumin level ($p < 0.001$), MELD score ($p < 0.001$), and LS ($p < 0.001$) among the three groups.

Liver-Related Events in Patients with Advanced Chronic Liver Disease

During the median follow-up period of 104 months (range, 11–117 months), hepatic decompensation occurred in 42 (22.6%) of the 186 patients in the cACLD group, with an annual incidence of 3.2% (95% confidence interval [CI], 2.4–4.4). The initial decompensating event was ascites in 17 (40.5%) patients, variceal bleeding in 15 (35.7%), and hepatic encephalopathy in 10 (23.8%). Liver-related death or liver transplantation occurred in 26 (14.0%) patients in the cACLD group (annual incidence, 1.9%; 95% CI, 1.3–2.8) and in 27 (43.5%) of the 62 patients in the dACLD group (annual incidence, 6.8%; 95% CI, 4.6–9.9). HCC developed in 44 (23.7%) patients in the cACLD group 18–112 (median, 59) months after the baseline and in 13 (21.0%) patients in dACLD group 26–104 (median, 67) months after the baseline.

Prediction of Hepatic Decompensation in the cACLD Group

The baseline multivariable model demonstrated that the baseline LS-SIR (sub-distribution hazard ratio [sHR], 0.81; 95% CI, 0.67–0.98; $p = 0.034$) and LS-VR (sHR, 0.71; 95% CI, 0.54–0.92; $p = 0.010$) were independently associated with hepatic decompensation along with sex and LS (Table 2). The optimal cutoff values of the baseline LS-SIR and LS-VR for predicting hepatic decompensation were 1.43 and 1.99, respectively. When the baseline LS-SIR and LS-VR cutoffs were combined, the patients were stratified into three distinct prognosis subgroups: high-risk (LS-SIR ≤ 1.43 and LS-VR ≤ 1.99; n = 11), intermediate-risk (one of LS-SIR ≤ 1.43 or LS-VR ≤ 1.99; n = 57), and low-risk (LS-SIR > 1.43 and LS-VR > 1.99; n = 118), with different CIFs of

https://doi.org/10.3348/kjr.2022.0494

Korean Journal of Radiology
KJR

hepatic decompensation (3-year, 36.4%, 11.1%, and 4.3%, respectively; 5-year, 54.6%, 19.4%, and 6.2%, respectively; $p < 0.001$ for all) (Fig. 2, Supplementary Table 1).

Among the 183 patients in the cACLD group, excluding the three patients who developed decompensation within 1 year after the baseline, the follow-up multivariable

Table 1. Characteristics of the Study Population

	Non-ACLD	cACLD	dACLD	*P*
Number of participants	32	186	62	
Age, years	57.2 ± 5.4	56.5 ± 8.3	56.7 ± 8.2	0.889
Male sex	15 (46.9)	103 (55.4)	35 (56.5)	0.063
Liver disease etiology				< 0.001
Hepatitis B	26 (81.3)	135 (72.6)	36 (58.1)	
Hepatitis C	4 (12.5)	20 (10.8)	3 (4.8)	
Alcohol	1 (3.1)	20 (10.8)	17 (27.4)	
Other	1 (3.1)	11 (5.9)	6 (9.7)	
Platelet, 10^9/L	82.0 ± 23.3	81.8 ± 31.2	70.6 ± 23.5	0.004
Albumin, g/dL	4.18 ± 0.33	3.94 ± 0.44	3.61 ± 0.50	< 0.001
MELD score	8.31 ± 1.84	9.70 ± 2.30	10.98 ± 2.33	< 0.001
LS, kPa*	7.3 (6.5–8.4)	13.8 (11.2–17.5)	18.6 (15.2–23.6)	< 0.001
Endoscopy				
Performed	7 (21.9)	87 (46.8)	44 (71.0)	
Varix present	0 (0)	54 (29.0)	38 (61.3)	
MRI index				
Baseline LS-SIR	1.84 ± 0.21	1.65 ± 0.22	1.52 ± 0.19	< 0.001
Baseline LS-VR	3.80 ± 2.33	3.18 ± 1.91	2.00 ± 1.04	< 0.001
ΔLS-SIR, %	3 ± 9	4 ± 8	3 ± 10	0.942
ΔLS-VR, %	1 ± 11	1 ± 12	1 ± 16	0.453

Unless otherwise indicated, data are presented as mean ± standard deviation or patient number with % in parentheses. *Data are median with interquartile ranges in parentheses. cACLD = compensated advanced chronic liver disease, dACLD = decompensated advanced chronic liver disease, LS = liver stiffness, LS-SIR = liver-to-spleen signal intensity ratio, ΔLS-SIR = changes in the LS-SIR in the 1-year follow-up MRI compared with that of the baseline MRI, LS-VR = liver-to-spleen volume ratio, ΔLS-VR = changes in LS-VR in the 1-year follow-up MRI compared with that in the baseline MRI, MELD = model for end-stage liver disease, Non-ACLD = non-advanced chronic liver disease

Table 2. Univariable and Multivariable Fine and Gray Regression Analysis for Factors associated with Hepatic Decompensation in Patients with Compensated Advanced Chronic Liver Disease

Variables	Univariable Analysis		Baseline Multivariable Model		Follow-Up Multivariable Model*	
	Sub-Distribution HR (95% CI)	*P*	Sub-Distribution HR (95% CI)	*P*	Sub-Distribution HR (95% CI)	*P*
Age (10-year increment)	1.13 (0.73–1.75)	0.588				
Male (compared with female)	2.63 (1.32–5.23)	0.006	3.49 (1.57–7.74)	0.002	2.60 (1.01–6.65)	0.047
Platelet (10 x 10^9/L increment)	1.01 (0.87–1.17)	0.919				
Albumin, g/dL	0.28 (0.14–0.56)	< 0.001	0.45 (0.19–1.09)	0.076	0.59 (0.21–1.63)	0.310
MELD	1.26 (1.13–1.41)	< 0.001	0.92 (0.76–1.13)	0.439	1.05 (0.87–1.27)	0.611
LS, kPa	1.02 (1.00–1.04)	0.030	1.04 (1.02–1.05)	< 0.001	1.03 (1.01–1.05)	0.002
Baseline LS-SIR	0.75 (0.65–0.86)	< 0.001	0.81 (0.67–0.98)	0.034	0.80 (0.64–0.99)	0.037
Baseline LS-VR	0.70 (0.57–0.88)	0.002	0.71 (0.54–0.92)	0.010	0.81 (0.60–1.10)	0.179
ΔLS-SIR (10% increment)	0.95 (0.63–1.43)	0.798			0.85 (0.49–1.47)	0.562
ΔLS-VR (10% increment)	0.46 (0.32–0.66)	< 0.001			0.54 (0.36–0.80)	0.002

Unless otherwise indicated, sub-distribution HRs are presented per one-unit increment of variable value. *Data were obtained from 183 patients after excluding three patients who developed hepatic decompensation within 1 year after the baseline examination. CI = confidence interval, HR = hazard ratio, LS = liver stiffness, LS-SIR = liver-to-spleen signal intensity ratio, ΔLS-SIR = changes in the LS-SIR in the 1-year follow-up MRI compared with that of the baseline MRI, LS-VR = liver-to-spleen volume ratio, ΔLS-VR = changes in LS-VR in the 1-year follow-up MRI compared with that in the baseline MRI, MELD = model for end-stage liver disease

https://doi.org/10.3348/kjr.2022.0494

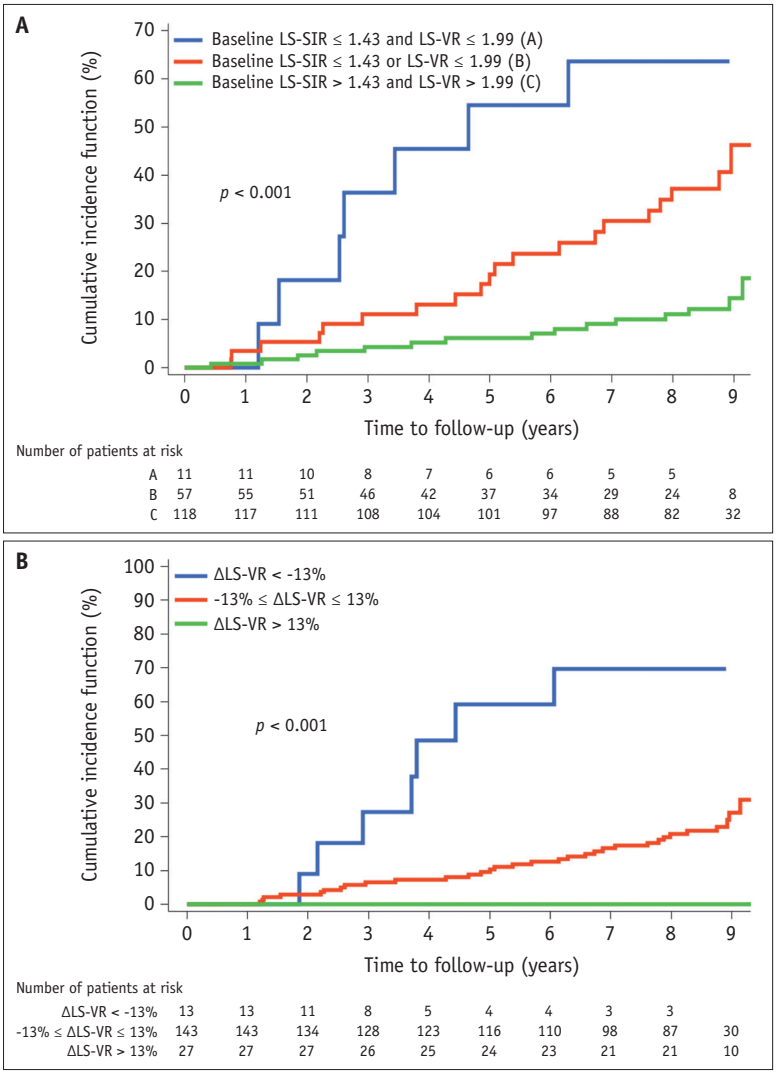

Fig. 2. Risks of hepatic decompensation in patients with compensated advanced chronic liver disease. The cumulative incidence function (%) of developing hepatic decompensation is estimated after accounting for competing events (death or liver transplantation) according to the combination of baseline LS-SIR and LS-VR **(A)** and the ΔLS-VR **(B)**. LS-SIR = liver-to-spleen signal intensity ratio, LS-VR = liver-to-spleen volume ratio, ΔLS-VR = changes in LS-VR in the 1-year follow-up MRI compared with that in the baseline MRI

model demonstrated that ΔLS-VR (sHR, 0.54 per 0.1-point increment in ΔLS-VR; 95% CI, 0.36–0.80; p = 0.002) was predictive of hepatic decompensation (Table 2). Using the predetermined cutoff values of ± 13%, ΔLS-VR classified the patients into three subgroups: ΔLS-VR < -13% (n = 13), -13% ≤ ΔLS -VR ≤ 13% (n = 143), and ΔLS -VR > 13% (n = 27), with 3-year and 5-year CIF of decompensation of 27.3%, 6.7%, and 0%, respectively, and 50.0%, 3.5%, and 0%, respectively (p < 0.001 for all) (Fig. 2, Supplementary Table 1). When ΔLS-VR was used in combination with baseline LS-SIR and LS-VR, ΔLS-VR allowed further division of the subgroups stratified by baseline LS-SIR and LS-VR (p < 0.001), as shown in Supplementary Figure 2 and Supplementary Table 1.

In the regression models including the development of HCC as the time-dependent covariate, MRI indices were still significantly associated with hepatic decompensation (sHR = 0.81 [p = 0.036] and 0.71 [p = 0.015] for LS-SIR and LS-VR, respectively, in the baseline model and 0.8 [p = 0.046] and 0.56 [p = 0.003] for LS-SIR and ΔLS-VR, respectively, in the follow-up model) after adjusting for the effect of HCC development (sHR = 3.24 [p = 0.001] and 3.09 [p < 0.001] for the baseline and follow-up models, respectively) (Supplementary Table 2).

Prediction of Liver-Related Death or Liver Transplantation in the cACLD Group

In the cACLD group, baseline LS-SIR (p = 0.121) and LS-

https://doi.org/10.3348/kjr.2022.0494

Korean Journal of Radiology
KJR

Table 3. Univariable and Multivariable Fine and Gray Regression Analysis for Factors associated with Liver-Related Death or Transplantation in Patients with Compensated Advanced Chronic Liver Disease

Variables	Univariable Analysis		Baseline Multivariable Model		Follow-Up Multivariable Model	
	Sub-Distribution HR (95% CI)	*P*	Sub-Distribution HR (95% CI)	*P*	Sub-Distribution HR (95% CI)	*P*
Age (10-year increment)	1.30 (0.77–2.22)	0.325				
Male (compared with female)	1.65 (0.74–3.65)	0.219				
Platelet (10 x 10^9/L increment)	1.00 (0.91–1.10)	0.964				
Albumin, g/dL	0.39 (0.16–0.93)	0.034	0.74 (0.21–2.70)	0.653	0.88 (0.26–2.91)	0.829
MELD	1.15 (1.02–1.30)	0.025	1.00 (0.83–1.21)	0.991	1.05 (0.87–1.26)	0.609
LS, kPa	1.02 (1.00–1.04)	0.057	1.03 (1.00–1.05)	0.029	1.01 (0.99–1.04)	0.271
Baseline LS-SIR	0.80 (0.69–0.91)	0.001	0.85 (0.69–1.05)	0.121	0.83 (0.66–1.04)	0.097
Baseline LS-VR	0.84 (0.61–1.16)	0.295	0.88 (0.58–1.32)	0.535	0.95 (0.61–1.48)	0.810
ΔLS-SIR (10% increment)	0.80 (0.48–1.32)	0.377			0.72 (0.43–1.21)	0.214
ΔLS-VR (10% increment)	0.41 (0.21–0.83)	0.013			0.46 (0.23–0.91)	0.026

Unless otherwise indicated, sub-distribution HRs are presented per one-unit increment of variable value. CI = confidence interval, HR = hazard ratio, LS = liver stiffness, LS-SIR = liver-to-spleen signal intensity ratio, ΔLS-SIR = changes in the LS-SIR in the 1-year follow-up MRI compared with that of the baseline MRI, LS-VR = liver-to-spleen volume ratio, ΔLS-VR = changes in LS-VR in the 1-year follow-up MRI compared with that in the baseline MRI, MELD = model for end-stage liver disease

VR (p = 0.535) were not significantly associated with the development of liver-related death or transplantation in the multivariable analysis (Table 3). When the follow-up MR indices were added to the baseline model, the follow-up multivariable model revealed that ΔLS-VR was the only significant predictor of liver-related death or transplantation, with an sHR of 0.46 (95% CI, 0.23–0.91; p = 0.026) (Table 3). As shown in Figure 3 and Supplementary Table 3, the patient subgroups stratified using the ΔLS-VR cutoffs of ± 13% showed different risks of liver-related death or transplantation (p < 0.001), with a 5-year CIF of 42.3%, 3.0%, and 0% for ΔLS-VR < -13% (n = 13), -13% ≤ ΔLS-VR ≤ 13% (n = 146), and ΔLS-VR > 13% (n = 27), respectively. In the multivariable models, including HCC development (Supplementary Table 4), ΔLS-VR did not show a statistically significant association with liver-related death or transplantation (HR = 0.52 [p = 0.060]) after adjusting for the effect of HCC development (sHR = 7.1 [p < 0.001] and 6.20 [p < 0.001] for the baseline and follow-up models, respectively).

Prediction of Liver-Related Death or Liver Transplantation in the dACLD Group

In the dACLD group, the baseline multivariable model demonstrated that the baseline LS-SIR was independently associated with liver-related death or transplantation (sHR, 0.67; 95% CI, 0.47–0.96; p = 0.027) (Table 4). However, in the follow-up multivariable model, ΔLS-VR was the only MRI index predictive of liver-related death or transplantation (sHR, 0.61; 95% CI, 0.40–0.93; p = 0.023) (Table 4). Using the optimal cutoff LS-SIR value of 1.33 (p = 0.014) and the ΔLS-VR cutoff value of ± 13% (p < 0.001), patients could be stratified into subgroups with different cumulative incidences of liver-related death or transplantation (Fig. 3, Supplementary Table 5). The development of HCC was not significantly associated with liver-related death or transplantation in the dACLD group (p = 0.448 and 0.308, respectively, in the baseline and follow-up models), and ΔLS-VR remained predictive of liver-related death or liver transplantation (sHR, 0.60; p = 0.023) after adjusting for the effect of HCC development (Supplementary Table 6). Representative examples are shown in Figure 4.

Technical Performance of the Deep Learning-Assisted Evaluation of MRI Indices

Among the 560 MRI examinations analyzed, DLA generated segmentation errors that required radiologist corrections in 95 (17.0%) examinations (error rate: 10.9% [7/64], 16.7% [62/372], and 21.0% [26/124] in the non-ACLD, cACLD, and dACLD groups, respectively; p = 0.214). Most segmentation errors were minor, which could be corrected in a short time (mean time for correction, 17.5 ± 9.7 seconds; range, 10–60 seconds) and were associated with a small change in the LS-SIR (95% limit of agreement, -1.2% to 1.3%) and LS-VR (95% limit of agreement, -6.8% to 5.7%). Patient categorization using the cutoff values for LS-SIR, LS-VR, and ΔLS-VR was concordant between the measurements by DLA and those after radiologist correction in 96.8% to 100% of patients (Supplementary Table 7).

 https://doi.org/10.3348/kjr.2022.0494

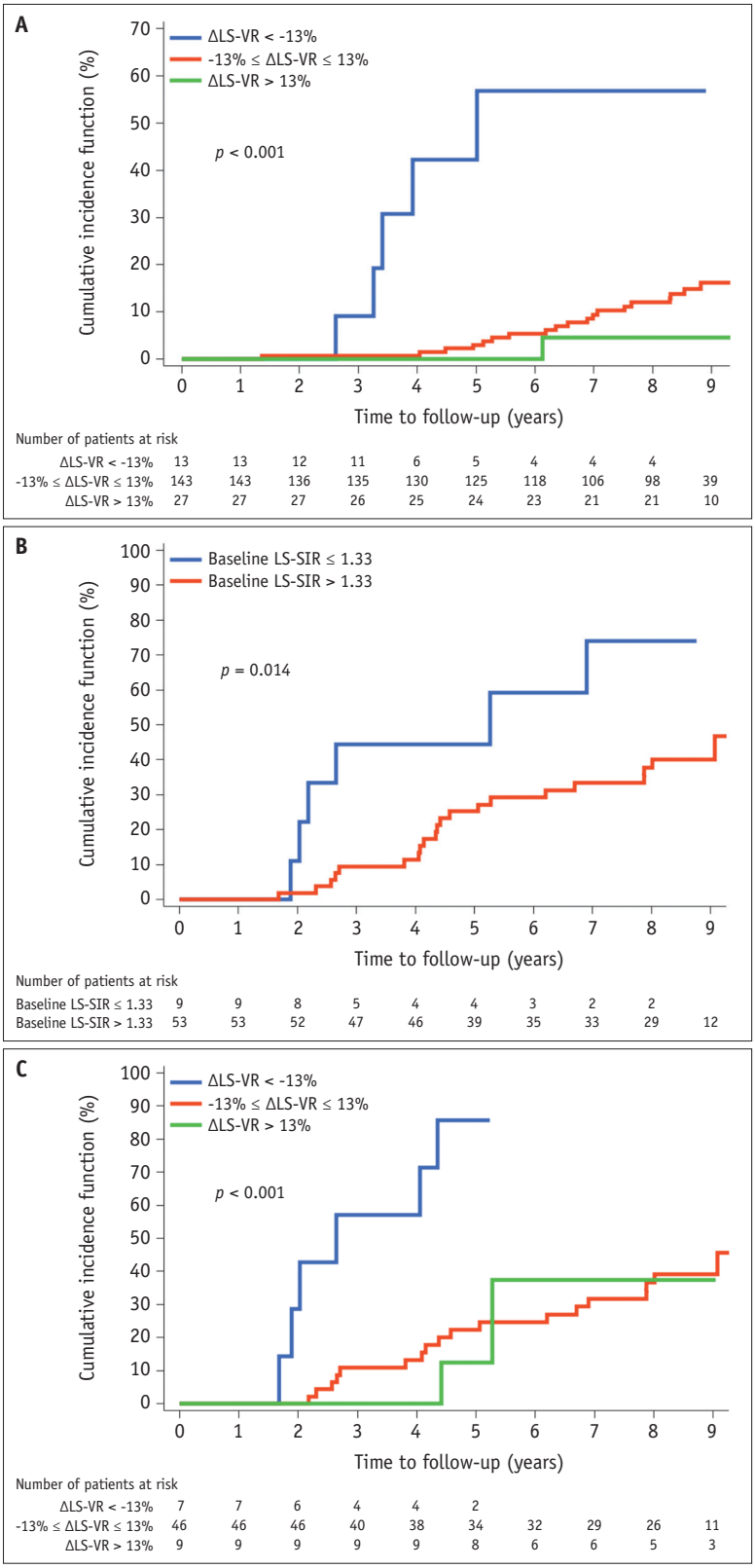

Fig. 3. Risks of liver-related death or transplantation. The cumulative incidence function (%) of liver-related death or transplantation was estimated after accounting for competing events (non-liver-related death) in patients with compensated advanced chronic liver disease according to ΔLS-VR **(A)** and in patients with decompensated advanced chronic liver disease according to baseline LS-SIR **(B)** and ΔLS-VR **(C)**. LS-SIR = liver-to-spleen signal intensity ratio, LS-VR = liver-to-spleen volume ratio, ΔLS-VR = changes in LS-VR in the 1-year follow-up MRI compared with that in the baseline MRI

https://doi.org/10.3348/kjr.2022.0494

Korean Journal of Radiology
KJR

Table 4. Univariable and Multivariable Fine and Gray Regression Analysis for Factors associated with Liver-Related Death or Transplantation in Patients with Decompensated Advanced Chronic Liver Disease

Variables	Univariable Analysis		Baseline Multivariable Model		Follow-Up Multivariable Model	
	Sub-Distribution HR (95% CI)	*P*	Sub-Distribution HR (95% CI)	*P*	Sub-Distribution HR (95% CI)	*P*
Age (10-year increment)	0.91 (0.59–1.40)	0.670				
Male (compared with female)	1.46 (0.68–3.11)	0.331				
Platelet (10 x 10^9/L increment)	1.10 (0.94–1.30)	0.244				
Albumin, g/dL	0.23 (0.11–0.48)	< 0.001	0.18 (0.08–0.42)	< 0.001	0.14 (0.05–0.36)	< 0.001
MELD	1.14 (0.98–1.33)	0.081	0.77 (0.58–1.02)	0.065	0.83 (0.64–1.07)	0.157
LS, kPa	1.03 (0.99–1.07)	0.129				
Baseline LS-SIR	0.74 (0.59–0.93)	0.009	0.67 (0.47–0.96)	0.027	0.70 (0.47–1.04)	0.080
Baseline LS-VR	0.83 (0.51–1.36)	0.470	0.70 (0.34–1.42)	0.320	0.88 (0.50–1.56)	0.670
ΔLS-SIR (10% increment)	0.96 (0.68–1.35)	0.802			1.12 (0.76–1.65)	0.561
ΔLS-VR (10% increment)	0.70 (0.46–1.05)	0.081			0.61 (0.40–0.93)	0.023

Unless otherwise indicated, sub-distribution HRs are presented per one-unit increment of variable value. CI = confidence interval, HR = hazard ratio, LS = liver stiffness, LS-SIR = liver-to-spleen signal intensity ratio, ΔLS-SIR = changes in the LS-SIR in the 1-year follow-up MRI compared with that of the baseline MRI, LS-VR = liver-to-spleen volume ratio, ΔLS-VR = changes in LS-VR in the 1-year follow-up MRI compared with that in the baseline MRI, MELD = model for end-stage liver disease

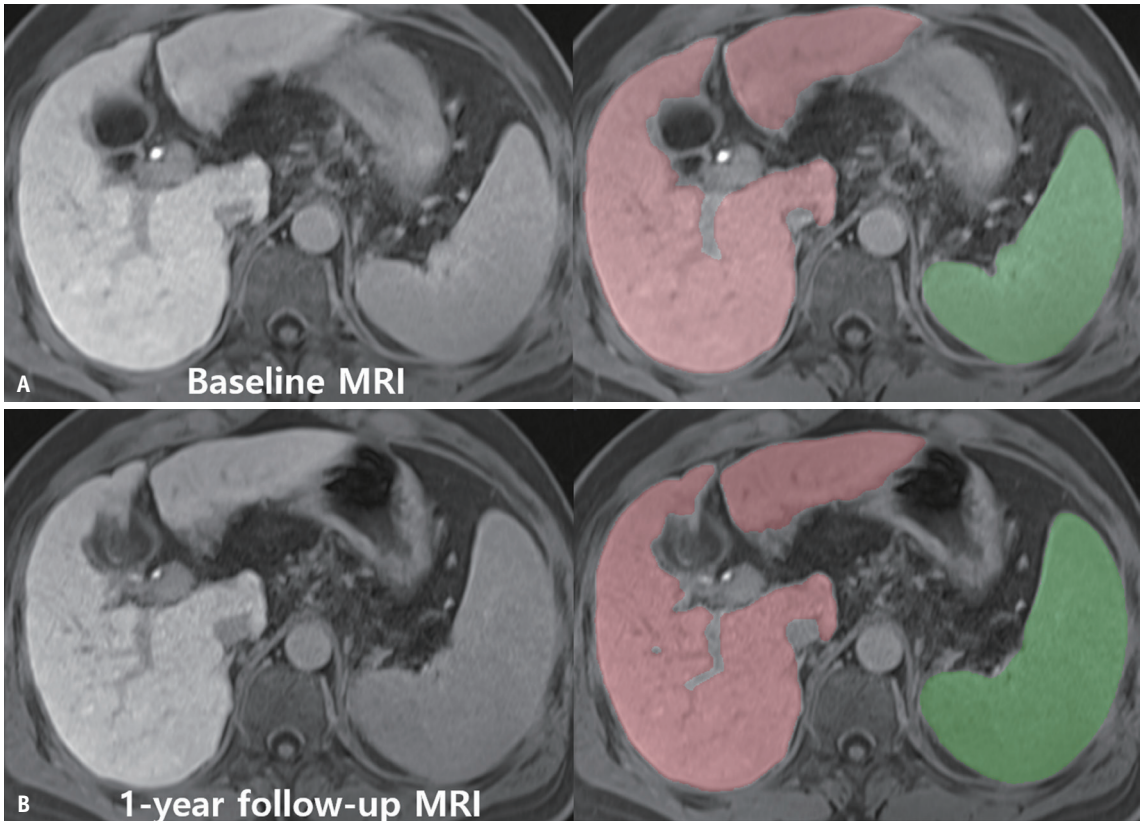

Fig. 4. Gadoxetic acid-enhanced hepatobiliary phase MR images in a 63-year-old male with compensated advanced chronic liver disease.

A, B. Axial hepatobiliary phase images at baseline **(A)** and 1-year **(B)** after baseline are presented with overlaid liver (pink) and spleen (green) masks generated using the deep learning algorithm. On baseline MRI, the LS-SIR was 1.34, and the liver and spleen volumes were 1153 cm^3 and 540 cm^3, respectively, resulting in a LS-VR of 2.86. On the 1-year follow-up MRI, LS-SIR and LS-VR were 1.43 and 1.61, respectively, with liver and spleen volumes of 1241 cm^3 and 773 cm^3, respectively. The ΔLS-VR between the baseline and 1-year follow-up MRI was -24.7%. The patient developed hepatic encephalopathy as the first decompensating event 25 months after the baseline examination and underwent liver transplantation 39 months after baseline examination. LS-SIR = liver-to-spleen signal intensity ratio, LS-VR = liver-to-spleen volume ratio, ΔLS-VR = changes in LS-VR in the 1-year follow-up MRI compared with that in the baseline MRI

https://doi.org/10.3348/kjr.2022.0494

DISCUSSION

Using the prospective cohort data of patients with ACLD who underwent baseline and 1-year follow-up liver MR examinations, this study demonstrated that the baseline LS-SIR and LS-VR predicted the risk of future hepatic decompensation in patients with cACLD, whereas the longitudinal change in LS-VR (i.e., ΔLS-VR) further stratified the decompensation risk and enabled the prediction of liver-related death or transplantation. Lower baseline LS-SIR (sHR = 0.81) and LS-VR (sHR = 0.71) were associated with a higher risk of hepatic decompensation, and a decrease in LS-VR during the 1-year follow-up period was associated with a higher risk of progression to decompensation (sHR = 0.54) and the composite endpoint of liver-related death or transplantation (sHR = 0.46). Similarly, in patients with dACLD, ΔLS-VR was predictive of liver-related death or transplantation, along with the baseline LS-SIR. Notably, the associations of LS-SIR, LS-VR, and ΔLS-VR with liver-related events were independent of LS and MELD, suggesting that these MRI-derived indices may provide incremental information in addition to the prognostic markers already used in clinical practice.

LS-SIR and LS-VR capture the different pathophysiological aspects of chronic liver disease. LS-SIR primarily reflects liver function [9-11], whereas LS-VR likely reflects the severity of liver fibrosis and portal hypertension [12,13]. Consistent with our findings, previous studies have reported the usefulness of LS-VR measured on CT in predicting hepatic decompensation or survival in patients with primary biliary cirrhosis [24] and hepatitis B cirrhosis [25]. However, the association between longitudinal changes in LS-VR and liver-related events has not been evaluated. We found that a cutoff ΔLS-VR value of ± 13% could categorize patients into distinct subgroups with different risks of hepatic decompensation and different risks of liver-related death or transplantation. More importantly, ΔLS-VR further stratified the decompensation risk groups using baseline MRI indices. Notably, regardless of the baseline LS-SIR and LS-VR values, none of the patients with cACLD with > 13% increase in ΔLS-VR during the 1-year follow-up developed any liver-related event. Thus, the longitudinal change in LS-VR could be a useful index for risk reassessment using follow-up MRI examinations.

Different approaches have been used to predict the prognosis of patients with chronic liver disease using gadoxetic acid-enhanced MRI, including visually assessed functional liver imaging scores [26] and volumetric liver T1 mapping [27]. Compared with these methods, the proposed approach has potential advantages. Compared with volumetric liver T1 mapping, which may not be available with some MRI scanners, our approach based on routine HBP images would be better for clinical application. Furthermore, using DLA for liver and spleen segmentation enabled automated measurement of MRI-derived indices, with rapidly correctable minor errors (< 7% of measured values) being observed in only 17% of MR examinations. Thus, the DLA facilitates the clinical application of LS-SIR, LS-VR, and ΔLS-VR, thereby adding information on the risk of liver-related events to routine gadoxetic acid-enhanced MRI. ΔLS-VR would be particularly useful for patients undergoing repeated gadoxetic acid-enhanced MRI examination for HCC surveillance or follow-up of hepatic lesions, as it allows reassessment of the risk of liver-related events at each follow-up time point.

Our study had some limitations. First, as our study population was derived from a prospective cohort of patients with a high risk of developing HCC and those who underwent MRI-based surveillance, it may not accurately represent the general population with ACLD. The generalizability of our findings requires further validation. Second, hepatitis B was the most common cause of liver disease in our study population. Thus, our findings require further validation in patients with liver disease due to other etiologic causes. Third, a threshold of ± 13% for ΔLS-VR was chosen based on the reported reproducibility range of liver volume measurements [20], which may not address the measurement error range of LS-VR. To determine a reliable threshold for ΔLS VR, the reproducibility of MRI-based LS VR measurements needs to be determined in a future study. Finally, the number of patients, especially those with dACLD, was small, limiting the statistical power of our analyses.

In conclusion, quantitative MRI indices measured using gadoxetic acid-enhanced MRI can be used as prognostic markers for patients with ACLD. Lower baseline LS-SIR and LS-VR values were associated with a higher risk of hepatic decompensation. A decrease in LS-VR during the longitudinal follow-up was associated with disease progression to decompensation and a higher risk of liver-related death or transplantation. The use of DLA enables the automated measurement of MRI indices, facilitating their use for risk stratification of ACLD in clinical practice.

https://doi.org/10.3348/kjr.2022.0494

Korean Journal of Radiology
KJR

Supplement

The Supplement is available with this article at https://doi.org/10.3348/kjr.2022.0494.

Availability of Data and Material

The datasets generated or analyzed during the study are available from the corresponding author on reasonable request.

Conflicts of Interest

Seung Soo Lee and So Yeon Kim who is on the editorial board of the *Korean Journal of Radiology* was not involved in the editorial evaluation or decision to publish this article. All remaining authors have declared no conflicts of interest.

Author Contributions

Conceptualization: Seung Soo Lee. Data curation: Subin Heo, So Yeon Kim, Hyo Jung Park. Formal analysis: Ji Sung Lee. Funding acquisition: Seung Soo Lee. Investigation: Seung Soo Lee, Subin Heo. Methodology: Seung Soo Lee, Subin Heo. Project administration: Seung Soo Lee. Resources: So Yeon Kim, Young-Suk Lim, Yu Sub Sung, Bumwoo Park. Software: Jee Seok Yoon, Heung-Il Suk, Yu Sub Sung, Bumwoo Park. Supervision: Seung Soo Lee. Validation: Seung Soo Lee. Visualization: Subin Heo, Seung Soo Lee. Writing—original draft: Subin Heo. Writing—review & editing: Seung Soo Lee.

ORCID iDs

Subin Heo
https://orcid.org/0000-0002-4700-1014
Seung Soo Lee
https://orcid.org/0000-0002-5518-2249
So Yeon Kim
https://orcid.org/0000-0001-6853-8577
Young-Suk Lim
https://orcid.org/0000-0002-1544-577X
Hyo Jung Park
https://orcid.org/0000-0002-2364-9940
Jee Seok Yoon
https://orcid.org/0000-0003-0721-504X
Heung-Il Suk
https://orcid.org/0000-0001-7019-8962
Yu Sub Sung
https://orcid.org/0000-0002-9215-735X
Bumwoo Park
https://orcid.org/0000-0002-1651-364X
Ji Sung Lee
https://orcid.org/0000-0001-8194-3462

Funding Statement

This work was supported by the National Research Foundation of Korea (NRF) grant funded by the Korea government (MSIT) (NRF-2020R1F1A1048826).

REFERENCES

1. de Franchis R; Baveno VI Faculty. Expanding consensus in portal hypertension: report of the Baveno VI Consensus Workshop: stratifying risk and individualizing care for portal hypertension. *J Hepatol* 2015;63:743-752
2. D'Amico G, Garcia-Tsao G, Pagliaro L. Natural history and prognostic indicators of survival in cirrhosis: a systematic review of 118 studies. *J Hepatol* 2006;44:217-231
3. Shearer JE, Jones R, Parker R, Ferguson J, Rowe IA. The natural history of advanced chronic liver disease defined by transient elastography. *Clin Gastroenterol Hepatol* 2022 Mar 23 [Epub]. https://doi.org/10.1016/j.cgh.2022.03.015
4. Kim HD, Lim YS, Han S, An J, Kim GA, Kim SY, et al. Evaluation of early-stage hepatocellular carcinoma by magnetic resonance imaging with gadoxetic acid detects additional lesions and increases overall survival. *Gastroenterology* 2015;148:1371-1382
5. Lee YJ, Lee JM, Lee JS, Lee HY, Park BH, Kim YH, et al. Hepatocellular carcinoma: diagnostic performance of multidetector CT and MR imaging-a systematic review and meta-analysis. *Radiology* 2015;275:97-109
6. Kim HL, An J, Park JA, Park SH, Lim YS, Lee EK. Magnetic resonance imaging is cost-effective for hepatocellular carcinoma surveillance in high-risk patients with cirrhosis. *Hepatology* 2019;69:1599-1613
7. Kim SY, An J, Lim YS, Han S, Lee JY, Byun JH, et al. MRI with liver-specific contrast for surveillance of patients with cirrhosis at high risk of hepatocellular carcinoma. *JAMA Oncol* 2017;3:456-463
8. European Association for the Study of the Liver. EASL clinical practice guidelines: management of hepatocellular carcinoma. *J Hepatol* 2018;69:182-236
9. Asenbaum U, Ba-Ssalamah A, Mandorfer M, Nolz R, Furtner J, Reiberger T, et al. Effects of portal hypertension on gadoxetic acid-enhanced liver magnetic resonance: diagnostic and prognostic implications. *Invest Radiol* 2017;52:462-469
10. Yamada A, Hara T, Li F, Fujinaga Y, Ueda K, Kadoya M, et al. Quantitative evaluation of liver function with use of gadoxetate disodium-enhanced MR imaging. *Radiology* 2011;260:727-733
11. Park HJ, Yoon JS, Lee SS, Suk HI, Park B, Sung YS, et al. Deep

learning-based assessment of functional liver capacity using gadoxetic acid-enhanced hepatobiliary phase MRI. *Korean J Radiol* 2022;23:720-731
12. Iranmanesh P, Vazquez O, Terraz S, Majno P, Spahr L, Poncet A, et al. Accurate computed tomography-based portal pressure assessment in patients with hepatocellular carcinoma. *J Hepatol* 2014;60:969-974
13. Son JH, Lee SS, Lee Y, Kang BK, Sung YS, Jo S, et al. Assessment of liver fibrosis severity using computed tomography-based liver and spleen volumetric indices in patients with chronic liver disease. *Eur Radiol* 2020;30:3486-3496
14. Lee CM, Lee SS, Choi WM, Kim KM, Sung YS, Lee S, et al. An index based on deep learning-measured spleen volume on CT for the assessment of high-risk varix in B-viral compensated cirrhosis. *Eur Radiol* 2021;31:3355-3365
15. Suh CH, Kim SY, Kim KW, Lim YS, Lee SJ, Lee MG, et al. Determination of normal hepatic elasticity by using real-time shear-wave elastography. *Radiology* 2014;271:895-900
16. Paisant A, Lemoine S, Cassinotto C, de Lédinghen V, Ronot M, Irlès-Depé M, et al. Reliability criteria of two-dimensional shear wave elastography: analysis of 4277 measurements in 788 patients. *Clin Gastroenterol Hepatol* 2022;20:400-408.e10
17. Barr RG, Wilson SR, Rubens D, Garcia-Tsao G, Ferraioli G. Update to the society of radiologists in ultrasound liver elastography consensus statement. *Radiology* 2020;296:263-274
18. D'Amico G, Morabito A, D'Amico M, Pasta L, Malizia G, Rebora P, et al. Clinical states of cirrhosis and competing risks. *J Hepatol* 2018;68:563-576
19. Fine JP, Gray RJ. A proportional hazards model for the subdistribution of a competing risk. *J Am Stat Assoc* 1999;94:496-509
20. Mojtahed A, Núñez L, Connell J, Fichera A, Nicholls R, Barone A, et al. Repeatability and reproducibility of deep-learning-based liver volume and Couinaud segment volume measurement tool. *Abdom Radiol (NY)* 2022;47:143-151
21. Williams B, Mandrekar JN, Mandrekar SJ, Cha SS, Furth AF. *Finding optimal cutpoints for continuous covariates with binary and time-to-event outcomes*. Rochester, MN: Mayo Clinic 2006
22. Aalen O. Nonparametric estimation of partial transition probabilities in multiple decrement models. *Ann Statist* 1978;6:534-545
23. Gray RJ. A class of K-sample tests for comparing the cumulative incidence of a competing risk. *Ann Stat* 1988;16:1141-1154
24. Murata Y, Abe M, Hiasa Y, Azemoto N, Kumagi T, Furukawa S, et al. Liver/spleen volume ratio as a predictor of prognosis in primary biliary cirrhosis. *J Gastroenterol* 2008;43:632-636
25. Kwon JH, Lee SS, Yoon JS, Suk HI, Sung YS, Kim HS, et al. Liver-to-spleen volume ratio automatically measured on CT predicts decompensation in patients with B viral compensated cirrhosis. *Korean J Radiol* 2021;22:1985-1995
26. Bastati N, Beer L, Mandorfer M, Poetter-Lang S, Tamandl D, Bican Y, et al. Does the functional liver imaging score derived from gadoxetic acid-enhanced MRI predict outcomes in chronic liver disease? *Radiology* 2020;294:98-107
27. Yoon JH, Lee JM, Kim E, Okuaki T, Han JK. Quantitative liver function analysis: volumetric T1 mapping with fast multisection B1 inhomogeneity correction in hepatocyte-specific contrast-enhanced liver MR imaging. *Radiology* 2017;282:408-417

https://doi.org/10.3348/kjr.2022.0494